

*Annual Review of Marine Science*

# Global Air–Sea Fluxes of Heat, Fresh Water, and Momentum: Energy Budget Closure and Unanswered Questions

Lisan Yu

Department of Physical Oceanography, Woods Hole Oceanographic Institution, Woods Hole, Massachusetts 02543, USA; email: lyu@whoi.edu

Annu. Rev. Mar. Sci. 2019. 11:227–48

First published as a Review in Advance on August 29, 2018

The *Annual Review of Marine Science* is online at marine.annualreviews.org

<https://doi.org/10.1146/annurev-marine-010816-060704>

Copyright © 2019 by Annual Reviews.  
All rights reserved

## ANNUAL REVIEWS CONNECT

[www.annualreviews.org](http://www.annualreviews.org)

- Download figures
- Navigate cited references
- Keyword search
- Explore related articles
- Share via email or social media

## Keywords

global-ocean energy budget, global-ocean freshwater budget, air–sea heat flux, air–sea freshwater flux, wind stress, air–sea buoy measurements, atmospheric reanalysis, satellite observations

## Abstract

The ocean interacts with the atmosphere via interfacial exchanges of momentum, heat (via radiation and convection), and fresh water (via evaporation and precipitation). These fluxes, or exchanges, constitute the ocean-surface energy and water budgets and define the ocean's role in Earth's climate and its variability on both short and long timescales. However, direct flux measurements are available only at limited locations. Air–sea fluxes are commonly estimated from bulk flux parameterization using flux-related near-surface meteorological variables (winds, sea and air temperatures, and humidity) that are available from buoys, ships, satellite remote sensing, numerical weather prediction models, and/or a combination of any of these sources. Uncertainties in parameterization-based flux estimates are large, and when they are integrated over the ocean basins, they cause a large imbalance in the global-ocean budgets. Despite the significant progress that has been made in quantifying surface fluxes in the past 30 years, achieving a global closure of ocean-surface energy and water budgets remains a challenge for flux products constructed from all data sources. This review provides a personal perspective on three questions: First, to what extent can time-series measurements from air–sea buoys be used as benchmarks for

accuracy and reliability in the context of the budget closures? Second, what is the dominant source of uncertainties for surface flux products, the flux-related variables or the bulk flux algorithms? And third, given the coupling between the energy and water cycles, precipitation and surface radiation can act as twin budget constraints—are the community-standard precipitation and surface radiation products pairwise compatible?

## 1. INTRODUCTION

The ocean's role in climate is manifested in its ability to transport heat poleward and regulate climate variability through exchange of heat, fresh water, and momentum with the atmosphere (e.g., Trenberth & Caron 2001, Wunsch 2005, Stephens et al. 2012, Wild et al. 2013). The fluxes, or exchange, at the air-sea interface are fundamental processes for keeping the global climate system in balance with the incoming insolation at Earth's surface (Loeb et al. 2012, Trenberth et al. 2014). They are also a primary conduit for coupling and feedback between the ocean and atmosphere on a broad range of scales, from synoptic weather events to regional and global circulation systems (e.g., Drennan et al. 2007, Førre et al. 2012, Gulev & Belyaev 2012, Drijfhout et al. 2014, Soloviev et al. 2014). Uncertainties in air-sea fluxes challenge our ability to understand how the ocean interacts with the atmosphere to influence the climate patterns worldwide, and how the interaction can be represented in Earth system models to improve the prediction of extreme weather events at long lead times. Air-sea flux products with not only high quality but also continuous and consistent climate records are sought to serve the needs of ocean and climate communities for the characterization, attribution, and modeling of weather and climate variability in the atmosphere and ocean (e.g., WGASF 2000, Curry et al. 2004, Fairall et al. 2010, Gulev et al. 2010).

Significant progress has been made in the past four decades in understanding and measuring the turbulent motions near the air-sea boundary (e.g., breaking waves, turbulence, sea spray, rain, and surface films) and their cumulative effects on the rates of transports of heat, moisture, and momentum across the interface (e.g., Louis 1979, Large & Pond 1981, Andreas et al. 1995, DeCosmo et al. 1996, Edson et al. 1998, Grachev et al. 2003, Weller et al. 2008). The direct covariance (or eddy correlation) technique (Crawford et al. 1993) has so far been the only established means for direct flux measurements at sea (e.g., Edson et al. 1998, Landwehr et al. 2015). However, direct flux measurements are currently available only at a limited number of locations for limited durations, because the measurements of vertical winds as well as temperature and humidity fluctuations need to be conducted on specially designed ships or buoys to minimize the effects of flow distortion and turbulent injection induced by the moving platforms. Air-sea fluxes in numerical models and global data products are computed from flux parameterizations that link the microscale turbulent transfers to easily measured macroscale quantities such as near-surface wind, humidity, and temperature. Sophisticated parameterizations have been developed, including the inertial-dissipation method, which infers surface fluxes from spectral characteristics of the inertial subrange (Fairall & Larsen 1986); the mean flux-profile method, which utilizes the empirical relationships between surface fluxes and mean profiles (gradients) of observed quantities in the surface layer (Paulson et al. 1972, Blanc 1983); and the bulk aerodynamic method, which employs the Monin-Obukhov similarity theory (Monin & Obukhov 1954, Garratt 1977, Large & Pond 1981). The bulk approach provides scaling relationships between surface fluxes and profiles of mean variables in the surface layer, and it determines the transfer coefficients from either empirically derived flux profiles (Liu et al. 1979) or direct covariance experiments (Fairall et al. 1996, 2003; Edson et al. 2013).

Of all types of parameterizations, the bulk aerodynamic parameterization is and will continue to be significant for air-sea flux estimation due to its easy applicability. The required input information of near-surface meteorology is routinely available from voluntary observing ships (VOSS), satellite remote sensing, and numerical weather prediction models. The algorithm developed during the Tropical Ocean–Global Atmosphere (TOGA) Coupled Ocean–Atmosphere Response Experiment (COARE) (Fairall et al. 1996, 2003; Edson et al. 2013) represents the state of the art in accuracy (Brunke et al. 2003) and has been used widely in constructing global air-sea flux gridded products using satellite and ship observations.

Using bulk parameterization, one can approximate surface turbulent momentum, heat, and freshwater fluxes as

$$\tau_x = \rho c_d(U - U_s)(u - u_s), \quad 1.$$

$$\tau_y = \rho c_d(U - U_s)(v - v_s), \quad 2.$$

$$LH = \rho L_v c_e (U - U_s)(q_s - q_a), \quad 3.$$

$$SH = \rho c_p c_h (U - U_s)(T_s - T_a), \quad 4.$$

$$E = LH/\rho_w L_v, \quad 5.$$

where  $\tau_x$  and  $\tau_y$  are the zonal and meridional wind stress components, respectively;  $LH$  the latent heat flux;  $SH$  the sensible heat flux; and  $E$  the moisture flux. The input variables for calculating the fluxes represented by Equations 1–5 are the zonal wind component ( $u$ ), meridional wind component ( $v$ ), and wind speed ( $U$ ) at a reference height; ocean-surface current velocity ( $U_s$ ), zonal current ( $u_s$ ), and meridional current ( $v_s$ ), which are usually small; sea-surface temperature (SST) ( $T_s$ ); potential air temperature ( $T_a$ ) and specific humidity ( $q_a$ ) at a reference height; and saturation-specific humidity ( $q_s$ ) as a function of  $T_s$  and sea-level pressure. The other constants are the air density ( $\rho$ ), seawater density ( $\rho_w$ ), latent heat of vaporization [ $L_v$ , which is expressed as  $L_v = (2.501 - 0.00237 \times T_s) \times 1.0^6$ ], and isobaric specific heat ( $c_p$ , where “p” denotes specific heat at a constant pressure). The turbulent transfer coefficients for stress ( $c_d$ , where “d” denotes wind stress drag), latent heat ( $c_e$ , where “e” denotes evaporation), and sensible heat ( $c_h$ ) depend on wind speed, atmospheric stability, measurement height, surface roughness, surface wave height, and wave age (e.g., Charnock 1955, Drennan et al. 2003, Andreas et al. 2008, Edson et al. 2013). Bulk flux algorithms differ from each other mainly in how roughness length is parameterized under various wind speeds. Significant uncertainties in these coefficients remain (Zeng et al. 1998, Brunke et al. 2003), particularly under very weak wind ( $U < 4 \text{ m s}^{-1}$ ) (e.g., Chang & Grossman 1999) or storm-force ( $U > 24 \text{ m s}^{-1}$ ) conditions (e.g., Powell et al. 2003, Andreas et al. 2008).

Air-sea exchange at the ocean surface comes not only in the form of turbulent fluxes by evaporation ( $LH$ ) and conduction ( $SH$ ) but also by means of radiative fluxes by shortwave and longwave radiation. Evaporation releases not only latent heat but also water vapor (see Equations 3 and 5). Because of the large amount of latent heat exchange during a phase change to liquid water (approximately  $2.5 \times 10^6 \text{ J kg}^{-1}$  if the SST effect is small), the transport of water vapor is regarded as the energy transport. Therefore, the water cycle is closely linked to the energy cycle, with the atmospheric circulation acting as the linchpin connecting the atmosphere and the ocean. The energy (hereafter denoted by  $Q_{\text{net}}$ ) and freshwater (hereafter  $FW$ ) budgets over the global ocean surface are expressed as

$$Q_{\text{net}} = SW - LW - LH - SH, \quad 6.$$

$$FW = P - E + R, \quad 7.$$

where  $SW$  is the net downward shortwave radiation,  $LW$  the net upward longwave radiation,  $P$  the precipitation, and  $R$  the river runoff. Because the energy and water budgets are conserved

quantities,  $Q_{\text{net}}$  and  $FW$  must be close to zero when integrated over the global ocean on annual and long-term mean bases. However, all parameterization-based flux products that are constructed from either ship reports or satellite observations do not include the ice-covered polar regions due to the lack of reliable observations. In this regard, the globally averaged mean represents a mean over the global ice-free open ocean rather than the entire global ocean, and so the long-term mean average of  $Q_{\text{net}}$  should be closed not to exactly zero but to within  $2\text{--}3 \text{ W m}^{-2}$  (Serreze et al. 2007, Bengtsson et al. 2013).

The ability to close the energy and freshwater budgets at the ocean surface has become a test of the accuracy of gridded flux products (Isemer et al. 1989, Josey et al. 1999, Fairall et al. 2010, Gulev et al. 2010, Yu et al. 2013, von Schuckmann et al. 2016, Liu et al. 2017, Valdivieso et al. 2017). This review provides a personal perspective on leading issues that challenge the parameterization-based flux products in achieving energy and freshwater budget closures.

## 2. ENERGY AND FRESHWATER BUDGET CLOSURES AND LEADING ISSUES

### 2.1. Leading Issues

Flux products are known to have large uncertainties that stem from both the uncertainties in flux-related variables ( $u$ ,  $v$ ,  $U$ ,  $q_a$ ,  $T_a$ , and  $T_s$ ) and the uncertainties in estimates of transfer coefficients ( $c_d$ ,  $c_e$ , and  $c_h$ ) in the bulk flux algorithms (Isemer et al. 1989, Josey et al. 1999, Brunke et al. 2003, Valdivieso et al. 2017). Satellite observations represent major improvements over VOS observations owing to their unprecedented sampling frequencies, spatial resolution, and truly global coverage. Nonetheless, spaceborne sensors cannot resolve the thermal quantities ( $T_a$  and  $q_a$ ) at a few meters above the surface, because the measured radiation is emitted from relatively thick atmospheric layers rather than from a single level (Simonot & Gautier 1989, Schulz et al. 1993). A common approach is to retrieve  $T_a$  and  $q_a$  from satellite-observed total column-integrated water vapor using in situ measurements as reference (Liu 1988, Schlüssel et al. 1995), but the empirically based retrieval algorithm may overly simplify the dependence of the vertical distribution of water vapor content on atmospheric stability and the advection of the large-scale circulation (Esbensen et al. 1993). There are substantial biases in  $T_a$  and  $q_a$  retrievals that are regime dependent (Yu & Jin 2018), and these biases have been the leading source of error for satellite-based flux products (Curry et al. 2004, Jackson et al. 2006, Prytherch et al. 2014).

The accuracy requirement for  $Q_{\text{net}}$  is  $10 \text{ W m}^{-2}$  for flux applications on monthly to seasonal timescales (WCRP 1989, Webster & Lukas 1992, WGASF 2000, Weller et al. 2004, Bradley & Fairall 2007). If the goal is to detect long-term trends from a background of natural variability, then the accuracy requirement is at least one order of magnitude higher, at  $O(1 \text{ W m}^{-2})$  for  $Q_{\text{net}}$  and  $O(1 \text{ cm y}^{-1})$  for  $FW$ . Observationally based estimates show that the ocean has amassed more than  $3 \times 10^{23} \text{ J}$  of energy since 1960, which corresponds to a net heating of  $0.5\text{--}1 \text{ W m}^{-2}$  over the global surface (Hansen et al. 2005, Levitus et al. 2005, Lyman & Johnson 2013, Allan et al. 2014, Cheng et al. 2017). All parameterization-based flux products have difficulty closing the ocean heat budget within this limit. Ship-based climatological analyses show mean heat gains by the ocean of approximately  $30 \text{ W m}^{-2}$  or greater (Isemer et al. 1989, Large et al. 1997, Josey et al. 1999), and satellite-based products have a similar degree of imbalance (Liu et al. 2017). Some have assumed that the imbalance is caused by errors in various flux formulae, which can be corrected by proportional adjustment of the flux components (Isemer et al. 1989, da Silva et al. 1994, Large & Yeager 2009), while others have suggested that the significant source of error may come from various regional biases in flux-related variables. These biases may arise from the undersampling

of extreme conditions in regions such as the high latitudes and the western boundary currents (Josey et al. 1999), uncorrected biases in  $T_a$  and  $q_a$  (Jin et al. 2015), etc. Hence, the unbalanced flux products are often adjusted by using inverse analysis (Isemer et al. 1989) with hydrographic heat transport constraints to close the global-ocean energy budget (Grist & Josey 2003). More recently, attempts have been made to determine an unbiased  $Q_{\text{net}}$  by combining satellite-based net radiation at the top of the atmosphere and the divergence of vertically integrated horizontal atmospheric energy transports, using the global mean radiation at the top of the atmosphere from the Clouds and the Earth's Radiant Energy System–Energy Balanced and Filled (CERES-EBAF, hereafter referred to as CERES) product (Loeb et al. 2018), which is anchored to estimates of global mean ocean heat storage.

Despite the progress made since the work by Isemer et al. (1989) and Josey et al. (1999), the inability to close the ocean heat budget remains a common problem in parameterization-based products that are largely constructed from satellite observations. Among the fundamental issues that are yet to be answered, the following three are most critical. First, all flux products have been based on the assumption that a good comparison with high-quality independent measurements from air-sea buoys indicates accuracy and reliability. But if this assumption is true, then why can the energy budget not be closed even though the flux products are in good agreement with buoy measurements? Second, there seems to be a consensus that the primary source of the energy budget imbalance is the underestimation of  $LH$  by approximately 15%, using the inverse flux adjustment analysis (Isemer et al. 1989, Grist & Josey 2003) and the vertically integrated energy budget adjustment (Liu et al. 2017). Is the underestimation caused solely by biases in flux-related variables (such as  $q_a$ )? Or does the bulk flux parameterization also play a role? Third, the ocean energy and freshwater budgets are connected through  $LH$  (Equations 6 and 7), suggesting that the amount by which  $LH$  needs to be adjusted to close the energy budget can potentially be constrained using the ocean freshwater budget. Nowadays, the surface radiation product from CERES (Kato et al. 2013, Loeb et al. 2018) and the precipitation product from the Global Precipitation Climatology Project (GPCP) (Adler et al. 2003) have become community-standard products. Can they be paired to help diagnose the leading sources of uncertainties in parameterization-based turbulent flux products? These three issues are reviewed below.

## 2.2. Flux Products

Different products use different bulk formulae. All satellite-derived flux products (e.g., Chou et al. 1995; Kubota et al. 2002; Roberts et al. 2010; Andersson et al. 2011; Bentamy et al. 2013; Yu & Jin 2014, 2018) are established from the COARE bulk flux algorithms (Fairall et al. 1996, 2003; Edson et al. 2013). The ship-based turbulent flux climatology compiled by the National Oceanography Centre (NOC) (Josey et al. 1999, Berry & Kent 2011) is computed from the Smith (1988) algorithm. Atmospheric reanalyses have their own bulk parameterization schemes (Kalnay et al. 1996, Kanamitsu et al. 2002, Saha et al. 2010, Dee et al. 2011, Rienecker et al. 2011, Kobayashi et al. 2015, Molod et al. 2015). Surface flux products differ from each other because input data sources (satellites, VOS reports, and numerical weather prediction models) have uncertainties arising from at least one of the following deficiencies: incomplete global coverage, indirect satellite retrievals, systematic bias, and random error. Surface flux products are also sensitive to the choice of algorithms (e.g., Miller et al. 1992, Webster & Lukas 1992, Zeng et al. 1998, Brunke et al. 2003).

The Objectively Analyzed Air–Sea Fluxes (OAFlux) project at the Woods Hole Oceanographic Institution has been through two phases of flux product development. The first phase led to a 1°-gridded turbulent heat and moisture (i.e.,  $LH$ ,  $SH$ , and  $E$ ) flux analysis (hereafter

OAFlux-1×1), with  $q_a$  and  $T_a$  determined from objective synthesis of satellite-derived retrievals and atmospheric reanalyses and  $U$  from multiple satellite sensors (Yu & Weller 2007, Yu et al. 2008). The second phase of development has focused on constructing high-resolution (0.25°-gridded), full-range (i.e.,  $LH$ ,  $SH$ ,  $E$ ,  $\tau_x$ , and  $\tau_y$ ) turbulent flux products (hereafter OAFlux-HR), with flux-related variables determined solely from satellite retrievals (Jin & Yu 2013; Yu & Jin 2014, 2018). Compared with OAFlux-1×1 (Yu & Weller 2007, Yu et al. 2008), OAFlux-HR has made improvements in three main aspects: spatial resolution,  $q_a$  and  $T_a$  estimates, and the inclusion of momentum fluxes. The improvement leads to an increase of  $LH + SH$  by approximately 8 W m<sup>-2</sup>, but disappointingly, it does not lead to an energy budget closure. When combined with CERES surface radiation ( $SW - LW$ ), OAFlux-1×1  $LH + SH$  produces a mean heat gain of approximately 25 W m<sup>-2</sup> over the global ocean, while OAFlux-HR  $LH + SH$  has a gain of approximately 17 W m<sup>-2</sup>. Since CERES has been adjusted to balance Earth's energy budget, the imbalance once again points to uncorrected bias in OAFlux-HR. From the viewpoint of the flux variable estimation, this argument is not convincing. The OAFlux-HR satellite-derived variables ( $q_a$ ,  $T_a$ , and  $U$ ) have been thoroughly validated with in situ time series measurements at more than 120 locations. The mean biases relative to buoy measurements are  $-0.34\text{ g kg}^{-1}$  for  $q_a$  (i.e., a dry bias),  $-0.08^\circ\text{C}$  for  $T_a$  (i.e., a slight cold bias), and  $-0.13\text{ m s}^{-1}$  for  $U$  (i.e., a weak bias) (Yu & Jin 2012, 2018). A simple error diagnosis of the bulk formula for  $LH$  and  $SH$ , assuming a mean wind speed of 7 m s<sup>-1</sup>, suggests that the adjustment of the 17 W m<sup>-2</sup> imbalance requires the mean state of the near-surface air to be either further dried by 0.74 g kg<sup>-1</sup> or cooled by 0.46°C. The magnitude of adjustment is way beyond the product accuracy defined by buoy evaluation.

Uncertainty in the bulk flux algorithms is the only stone left unturned in our pursuit of surface energy budget closure. When comparing the two versions of OAFlux products with atmospheric reanalyses, the influence of bulk algorithms on surface flux estimates is evident. Hence, there is a need to understand the uncertainties in both flux-related variables and bulk algorithms to gain a complete understanding of the cause of the surface budget imbalance. Since all satellite-derived products are produced from COARE version 3 (v3), differences between products reflect the differences between variable estimation, which have been characterized by several comparison studies (Bentamy et al. 2017). To narrow the scope of this review, I limit the discussion to nine atmospheric reanalyses, three OAFlux products, and the ship-based NOC algorithm and use CERES and GPCP as budget constraints (**Table 1**).

The OAFlux-HR full-range turbulent flux products can be combined with CERES and GPCP to provide a complete description of ocean-surface heat, freshwater, and momentum fluxes. The annual-mean fields of  $Q_{\text{net}}$  are from CERES and OAFlux-HR, those of evaporation minus precipitation (hereafter  $E - P$ ) are from OAFlux-HR and GPCP, and those of wind stress vector and wind stress curl (i.e.,  $\partial\tau_y/\partial x - \partial\tau_x/\partial y$ ) are from OAFlux-HR in 2014 (**Figure 1**). Consistent with the climatological mean patterns (e.g., Josey et al. 2013), the tropical ocean is the primary region of atmospheric heat and freshwater input to the ocean, and the subtropical ocean (particularly the western boundary current regime) is the region of oceanic heat and freshwater transfer to the atmosphere. In the Northern Hemisphere, cyclonic (positive) wind stress curl drives an upward Ekman pumping and upwelling, while anticyclonic (negative) wind stress curl drives Ekman suction and downwelling. In the Southern Hemisphere, the effects are the opposite, with cyclonic (positive) wind stress curl denoting downwelling and anticyclonic (negative) wind stress curl denoting upwelling. Although CERES  $SW$  and  $LW$  are 1° gridded and GPCP precipitation is 2.5° gridded, the high-resolution advantage of OAFlux-HR in depicting the fine structure of frontal-scale air-sea exchanges is seen in the western boundary current regimes.

**Table 1 General characteristics of surface flux products used in this article (nine atmospheric reanalyses and four satellite- and ship-based products in addition to CERES and GPCP)**

Product	Period of availability	Temporal resolution	Grid spacing	Surface flux variables	Reference(s)
<b>Atmospheric reanalyses</b>					
NCEP1	1948–present	6 hourly	$1.875^\circ \times 1.875^\circ$	$SW, LW, LH, SH, E, P, \tau_x, \tau_y$	Kalnay et al. 1996
NCEP2	1979–present	6 hourly	$1.875^\circ \times 1.875^\circ$	$SW, LW, LH, SH, E, P, \tau_x, \tau_y$	Kanamitsu et al. 2002
CFSR	1979–present	Hourly	$0.5^\circ \times 0.5^\circ$	$SW, LW, LH, SH, E, P, \tau_x, \tau_y$	Saha et al. 2010
ERA-Interim	1979–present	6 hourly	$0.7^\circ \times 0.7^\circ$	$SW, LW, LH, SH, E, P, \tau_x, \tau_y$	Dee et al. 2011
MERRA	1979–present	3 hourly	$0.667^\circ \times 0.5^\circ$	$SW, LW, LH, SH, E, P, \tau_x, \tau_y$	Rienecker et al. 2011
MERRA-2	1980–present	Hourly	$0.625^\circ \times 0.5^\circ$	$SW, LW, LH, SH, E, P, \tau_x, \tau_y$	Molod et al. 2015
JRA-55	1958–present	3 hourly	$0.55^\circ \times 0.55^\circ$	$SW, LW, LH, SH, E, P, \tau_x, \tau_y$	Kobayashi et al. 2015
20CR	1950–2011	6 hourly	$2^\circ \times 2^\circ$	$SW, LW, LH, SH, E, P, \tau_x, \tau_y$	Compo et al. 2011
ERA-20C	1900–2010	3 hourly	$1.125^\circ \times 1.125^\circ$	$SW, LW, LH, SH, E, P, \tau_x, \tau_y$	Poli et al. 2013
<b>Satellite- and ship-based products</b>					
OAFlux-1×1	1958–present	Daily, monthly	$1^\circ \times 1^\circ$	$LH, SH, E$	Yu & Weller 2007
OAFlux-HR3	1988–present	Daily	$0.25^\circ \times 0.25^\circ$	$LH, SH, E, \tau_x, \tau_y$ [using bulk flux algorithm COARE v3 (Fairall et al. 2003)]	Yu & Jin 2014, 2018
OAFlux-HR4	1988–present	Daily	$0.25^\circ \times 0.25^\circ$	$LH, SH, E, \tau_x, \tau_y$ [using bulk flux algorithm COARE v4 (Edson 2008)]	Yu & Jin 2014, 2018
NOC	1976–2014	Monthly	$1^\circ \times 1^\circ$	$SW, LW, LH, SH$	Berry & Kent 2011
<b>Products used as budget constraints</b>					
CERES	2000–present	Daily	$1^\circ \times 1^\circ$	$SW, LW$	Loeb et al. 2018
GPCP	1979–present	Daily	$2.5^\circ \times 2.5^\circ$	$P$	Adler et al. 2003

Abbreviations: 20CR, Twentieth Century Reanalysis; CERES, Clouds and the Earth's Radiant Energy System—Energy Balanced and Filled; CFSR, Climate Forecast System Reanalysis; COARE v3 and v4, Coupled Ocean–Atmosphere Response Experiment version 3 and version 4, respectively; ERA-20C, European Centre for Medium-Range Weather Forecasts Twentieth Century; ERA-Interim, European Centre for Medium-Range Weather Forecasts Interim; GPCP, Global Precipitation Climatology Project; JRA-55, Japanese 55-Year Reanalysis; MERRA, Modern-Era Retrospective Analysis for Research and Applications; NCEP, National Center for Environmental Prediction; NOC, National Oceanography Centre; OAFlux-1×1, 1°-gridded Objectively Analyzed Air–Sea Fluxes; OAFlux-HR3 and -HR4, high-resolution ( $0.25^\circ$ -gridded) Objectively Analyzed Air–Sea Fluxes based on Coupled Ocean–Atmosphere Response Experiment (COARE) version 3 and version 4, respectively.

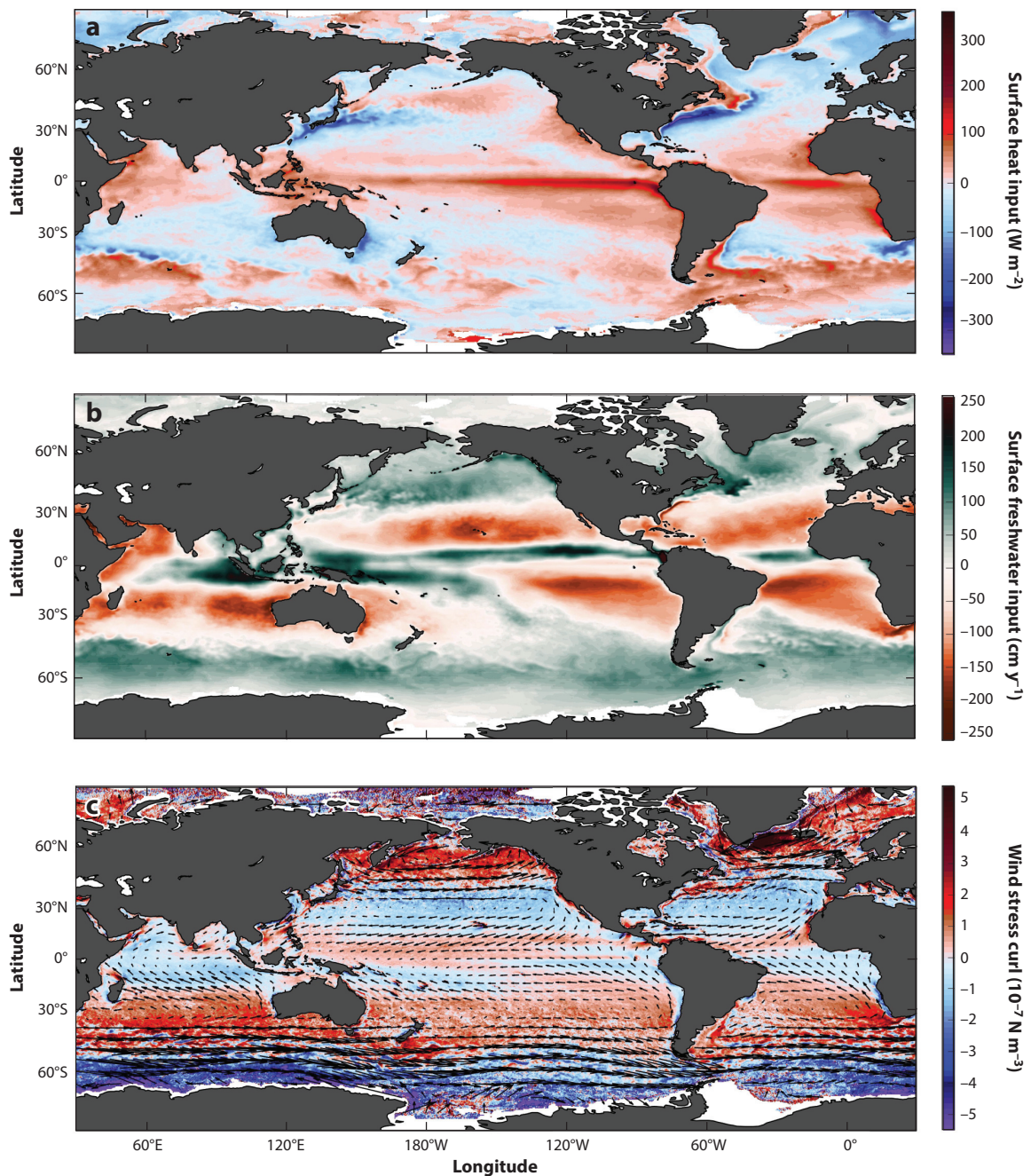


**Figure 1**

Annual-mean (a) surface heat input,  $Q_{\text{net}}$ , from CERES and OAFlux-HR4; (b) surface freshwater input,  $E - P$ , from OAFlux-HR4 and GPCP; and (c) wind stress vector (arrows) and wind stress curl (colors) in 2016. Abbreviations: CERES, Clouds and the Earth's Radiant Energy System—Energy Balanced and Filled; GPCP, Global Precipitation Climatology Project; OAFlux-HR4, high-resolution (0.25°-gridded) Objectively Analyzed Air–Sea Fluxes analysis computed from Coupled Ocean–Atmosphere Response Experiment (COARE) version 4.

### 2.3. Differences in Bulk Parameterization Algorithms

Unlike OAFlux- $1 \times 1$ , which is constructed from COARE v3, the OAFlux-HR flux fields in **Figure 1** are computed from the updated COARE v4 bulk flux algorithm (Edson 2008). COARE v4 has focused on improving turbulent transfer coefficients (Edson 2008), particularly  $c_e$  and  $c_h$  for *LH* and *SH* (J.B. Edson, personal communication). In COARE v3, the coefficients for *LH* and *SH* are identical, assuming similarity in the transfer of heat and mass. In COARE v4, *LH* and *SH* are modeled with separate formulae and validated with direct flux measurements from field programs. The  $c_e$  estimate in the two algorithms exhibits the same overall characteristics of a minimum around wind speeds of  $3\text{--}4\text{ m s}^{-1}$ ; after that,  $c_e$  in COARE v4 increases to a maximum around wind speeds of  $12\text{ m s}^{-1}$  before falling off at higher winds, while  $c_e$  in COARE v3 shows a near-linear increase with wind speed. In the following, OAFlux-HR computed from COARE v3 is denoted OAFlux-HR3, and OAFlux-HR computed from COARE v4 is denoted as OAFlux-HR4.

The zonal averages of the annual-mean *LH* + *SH* fields in 2014 from OAFlux-HR3, OAFlux-HR4, and OAFlux- $1 \times 1$  and their differences (**Figure 2a,b**) show that the three products differ most at low and middle latitudes. The differences between OAFlux-HR3 and OAFlux-HR4 reflect the change induced by the COARE algorithms, and COARE v4 produces stronger *LH* + *SH* at all latitudes, with maximum differences of approximately  $20\text{ W m}^{-2}$  at  $30\text{--}40^\circ\text{N/S}$ . The  $30\text{--}40^\circ\text{S}$  latitudes are the locations of strong turbulent heat loss associated with western boundary currents. The differences between OAFlux- $1 \times 1$  and OAFlux-HR3 reflect the change made in flux variables due to resolution change and the use of a satellite-only input data source, and the improvement leads to an average increase of approximately  $10\text{ W m}^{-2}$  for the latitudes between  $40^\circ\text{S}$  and  $40^\circ\text{N}$ . In general, COARE v3 is a weaker algorithm than COARE v4.

To assess the difference between COARE v3 and the bulk flux algorithms in reanalyses, the flux-related variables from the National Center for Environmental Prediction 1 (NCEP1), Climate Forecast System Reanalysis (CFSR), European Centre for Medium-Range Weather Forecasts Interim (ERA-Interim), and Modern-Era Retrospective Analysis for Research and Applications (MERRA) algorithms were used as input to COARE v3 to compute a set of COARE v3-based reanalysis fluxes. The zonally averaged mean differences between the original reanalysis fluxes and the COARE v3-based reanalysis fluxes in 2014 (**Figure 2c,d**) indicate that COARE v3 is a weak algorithm compared with the four reanalysis algorithms. The ERA-Interim algorithm is the closest to COARE v3, and the differences are mostly within  $5\text{ W m}^{-2}$  except for a  $10\text{ W m}^{-2}$  spike at approximately  $15^\circ\text{N/S}$ . The NCEP1 algorithm has the largest departure from COARE v3, with a magnitude approaching  $40\text{ W m}^{-2}$  at subtropical latitudes. The CFSR and MERRA algorithms are approximately 8 and  $12\text{ W m}^{-2}$  stronger, respectively, at most latitudes.

Bulk flux algorithms relate surface fluxes to flux-related variables through turbulent transfer coefficients. These coefficients are commonly parameterized as a function of atmospheric stability and surface roughness, with the latter being wind speed dependent in the COARE (Fairall et al. 2003, Edson et al. 2013), MERRA (Rienecker et al. 2011), NCEP1 (Kalnay et al. 1996), and CFSR (Saha et al. 2010) algorithms. On the other hand, the surface roughness in ERA-Interim (Janssen 2008) is parameterized as a function of the inverse wave age (Hwang 2005). Edson (2008) found that there is good agreement between the COARE v4 and ERA-Interim algorithms despite the differences in the two parameterizations. However, uncertainty remains about the behavior of the drag coefficient at the extreme wind conditions associated with tropical cyclones and hurricanes. When using the COARE v4 and ERA-Interim algorithms as a reference, the COARE v3 algorithm is on the weak side and the MERRA, NCEP1, and CFSR algorithms are on the strong side.

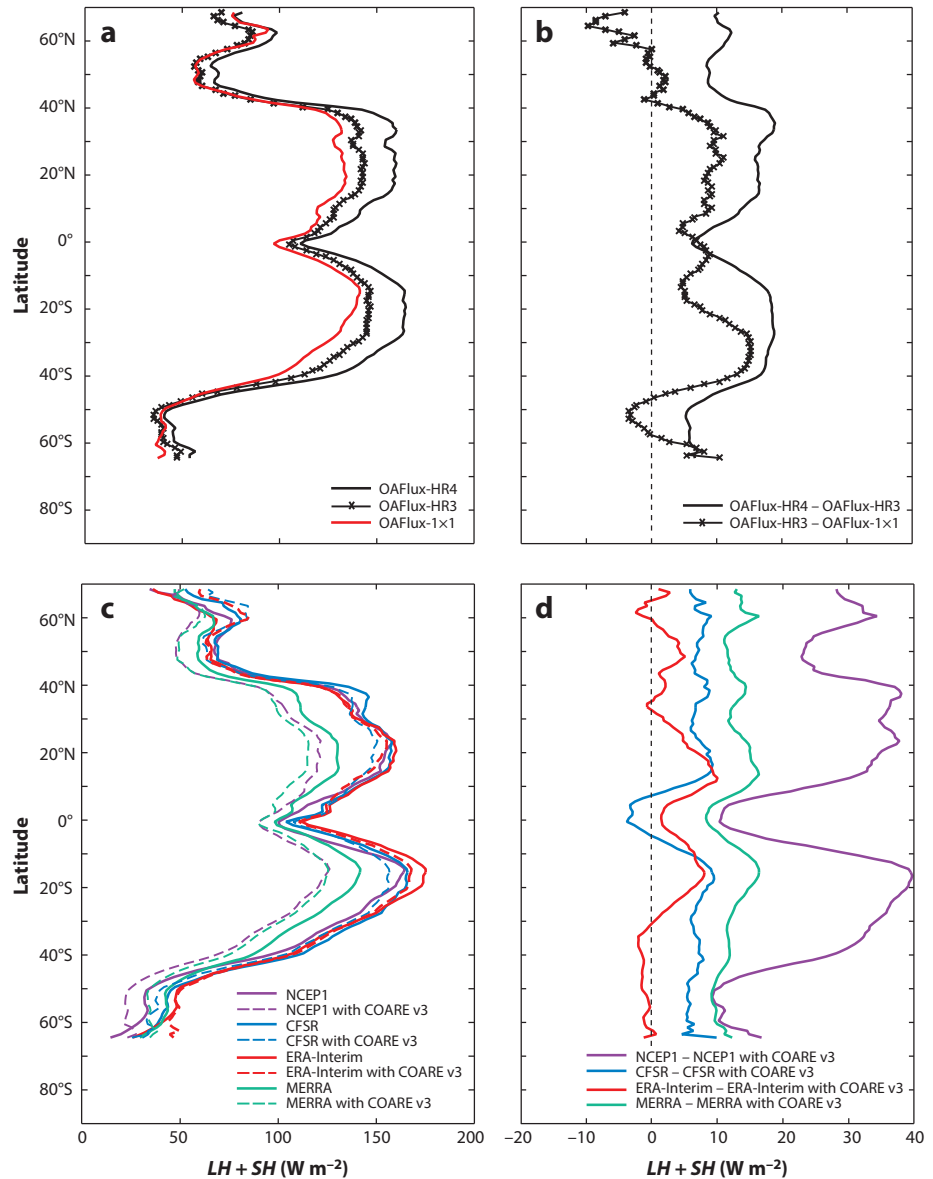


**Figure 2**

Zonally averaged mean  $LH + SH$  in 2014. (a) OAFlux-HR4, OAFlux-HR3, and OAFlux-1x1 products. (b) Differences between OAFlux-HR4 and OAFlux-HR3 and between OAFlux-HR3 and OAFlux-1x1. (c) Original NWP fluxes (solid lines) and recomputed fluxes using NWP variables as input to the COARE v3 algorithm (dashed lines). (d) Differences between the original NWP fluxes and the recomputed fluxes using NWP variables as input to the COARE v3 algorithm. Abbreviations: CFSR, Climate Forecast System Reanalysis; COARE v3, Coupled Ocean–Atmosphere Response Experiment version 3; ERA-Interim, European Centre for Medium-Range Weather Forecasts Interim; MERRA, Modern-Era Retrospective Analysis for Research and Applications; NCEP1, National Center for Environmental Prediction 1; NWP, numerical weather prediction; OAFlux-1x1, 1°-gridded Objectively Analyzed Air–Sea Fluxes; OAFlux-HR3 and -HR4, high-resolution ( $0.25^{\circ}$ -gridded) Objectively Analyzed Air–Sea Fluxes analysis computed from Coupled Ocean–Atmosphere Response Experiment (COARE) version 3 and version 4, respectively.

## 2.4. Interpretation of Buoy Evaluation

Time-series measurements from moored air-sea buoys in the global ocean serve as benchmarks for validating flux products constructed from various sources (Fairall et al. 2010, Gulev et al. 2010, Yu et al. 2013, Bentamy et al. 2017, Valdivieso et al. 2017). Despite good comparisons, none of flux products can achieve an energy budget closure without additional adjustments (e.g., Isemer et al. 1989, Josey et al. 1999). Two factors might be responsible for this. One is that buoy fluxes are not measured but computed (Weller et al. 2008), and the algorithm for buoy  $LH + SH$  is COARE v3. The computed buoy fluxes may not be bias free if there is uncertainty in the flux algorithm (**Figure 2**). The other is that the majority of buoys are deployed in the tropical warm-water zone, with a very limited number of buoys in the vicinity of western boundary currents and the high-latitude cold-water zone (**Figure 3a**).

To illustrate that COARE v3-based buoy fluxes may not be a viable verification for flux products, I computed daily-mean buoy fluxes (in terms of  $SW - LW$  and  $LH + SH$ ) that were acquired between 1990 and 2015 at 126 buoy locations (**Figure 3a**) and compared the results with collocated daily-mean CERES  $SW - LW$ , OAFlux- $1 \times 1$   $LH + SH$ , and six atmospheric reanalyses ( $SW - LW$  and  $LH + SH$ ). Since surface fluxes are a sensitive function of SST, I binned the product-minus-buoy flux differences onto  $0.5^{\circ}\text{C}$  SST grids using buoy observations. The distribution of product-minus-buoy differences with SST (**Figure 3b,c**) indicates that there are some exceptionally large values in a few SST regimes: low SSTs ( $<6^{\circ}\text{C}$ ), SSTs of  $15\text{--}20^{\circ}\text{C}$ , and very high SSTs ( $>30^{\circ}\text{C}$ ). The number of available buoy measurements is limited (less than 50) in these SST ranges such that the performance of flux products may not be statistically well represented. Away from these ranges, the errors in reanalysis  $SW - LW$  increase sharply for SSTs greater than  $20^{\circ}\text{C}$ , which correspond with the tropical/subtropical warm-water regime. Only satellite-derived CERES  $SW - LW$  is unbiased. As for the error distribution in  $LH + SH$ , all reanalyses have a similar error distribution pattern: The errors are smaller when SST is less than  $15^{\circ}\text{C}$  and larger when SST is greater than  $20^{\circ}\text{C}$ . Except for NCEP1 and MERRA, the errors remain more or less constant for SSTs of  $20\text{--}28^{\circ}\text{C}$ , although the magnitudes vary. The Japanese 55-Year Reanalysis (JRA-55) differs by more than  $40 \text{ W m}^{-2}$ , ERA-Interim differs by  $20 \text{ W m}^{-2}$ , and CFSR differs by  $17 \text{ W m}^{-2}$ . OAFlux- $1 \times 1$  is largely unbiased, but it is computed from COARE v3, the same algorithm used by buoy fluxes. Given that COARE v3 is weaker than the reanalysis algorithms (**Figure 2c,d**), it is yet to be determined which is a more dominant source of uncertainty for  $LH + SH$  products, the bulk algorithm or the flux-related variables.

## 2.5. Differences in Long-Term Mean Fields

The standard deviations between 12 mean  $Q_{\text{net}}$  products (**Table 1**) averaged over the overlapping 10-year period of 2001–2010 convey the same message that surface heat flux estimates are most uncertain in the tropical and subtropical regions (**Figure 4a**). In the Indo-Pacific warm pool, for instance, the standard-deviation differences between products exceed  $30 \text{ W m}^{-2}$ , which is greater than the ensemble mean of the products. Zonal averages of the 10-year mean  $Q_{\text{net}}$ ,  $SW - LW$ , and  $LH + SH$  (**Figure 4b-d**) indicate that JRA-55  $Q_{\text{net}}$  is an outlier, as its  $LH + SH$  is excessively strong in the tropics. OAFlux-HR4 is in the same range as reanalysis  $LH + SH$  at  $25\text{--}45^{\circ}\text{N/S}$  but is stronger than the reanalysis at midlatitudes because the high resolution of OAFlux-HR4 can better resolve the  $LH + SH$  associated with the western boundary current fronts.

The standard-deviation differences between 11 mean  $E - P$  products averaged over 2001–2010 (**Figure 5a-c**) are most pronounced in the tropical/subtropical regions between  $30^{\circ}\text{S}$  and  $30^{\circ}\text{N}$ . One major uncertainty is the spread in  $P$  products in regions of the Intertropical Convergence Zone and South Pacific Convergence Zone, with the satellite-based GPCP having the weakest

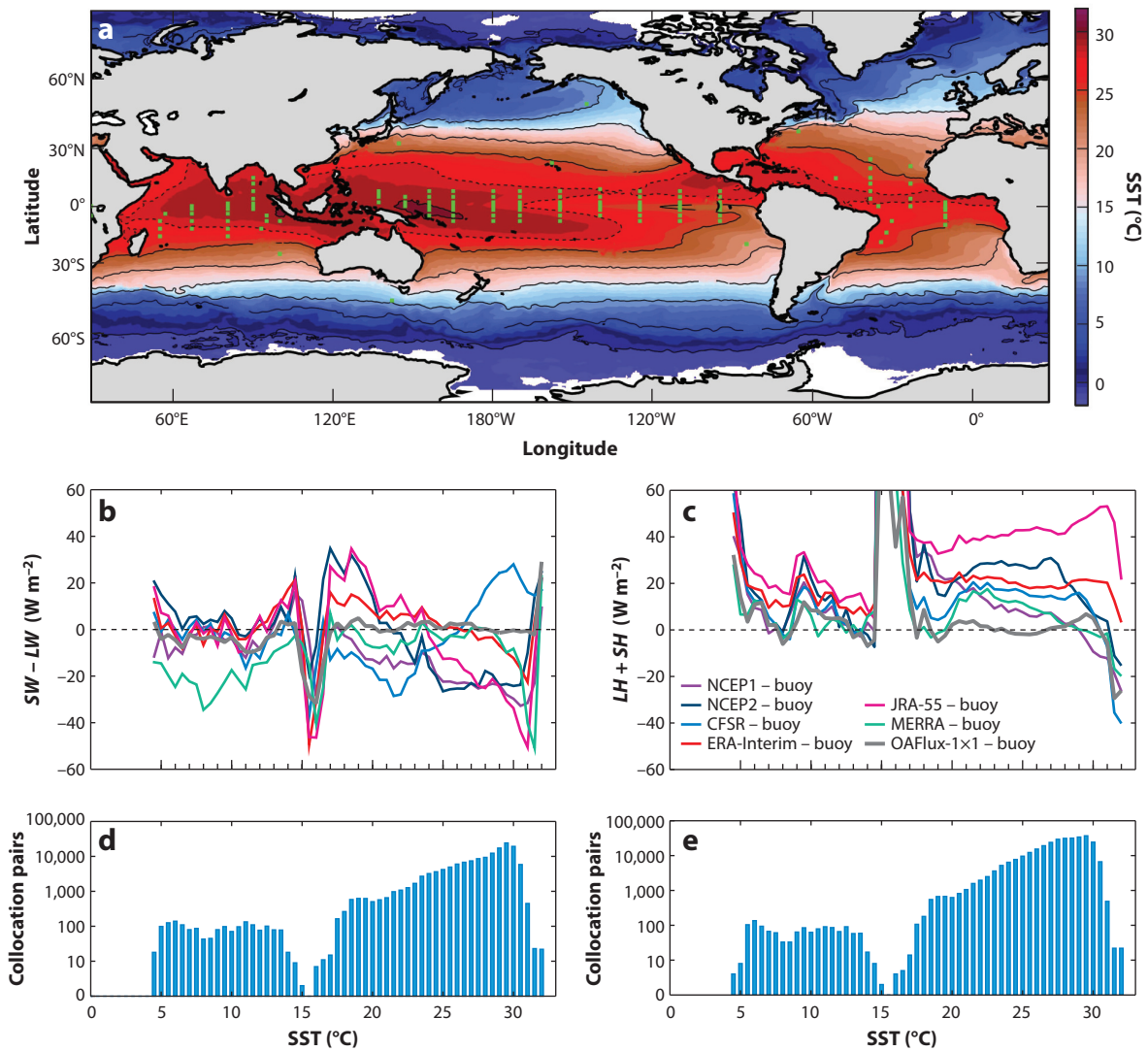


**Figure 3**

(a) Mean SST field in 2014 superimposed with locations of 126 buoys. (b) Distribution of product-minus-buoy differences in  $SW - LW$  with SST. (c) Distribution of product-minus-buoy differences in  $LH + SH$  with SST. (d) Number of buoy–product collocation pairs for daily-mean  $SW - LW$ . (e) Number of buoy–product collocation pairs for daily-mean  $LH + SH$ . Abbreviations: CFSR, Climate Forecast System Reanalysis; ERA-Interim, European Centre for Medium-Range Weather Forecasts Interim; JRA-55, Japanese 55-Year Reanalysis; MERRA, Modern-Era Retrospective Analysis for Research and Applications; NCEP, National Center for Environmental Prediction; SST, sea-surface temperature.

rainfall and JRA-55 the strongest rainfall. The pattern of differences suggests that reanalyses have difficulty in simulating tropical convective clouds and rainfall processes (Rosenfeld & Lensky 1998, Newman et al. 2000, Yu et al. 2017). In contrast to the standard-deviation  $E - P$  pattern, the standard-deviation differences between 11 mean wind stress magnitude ( $\tau$ ) products averaged over 2001–2010 show that large deviations are located at mid-to-high latitudes where winds are strong

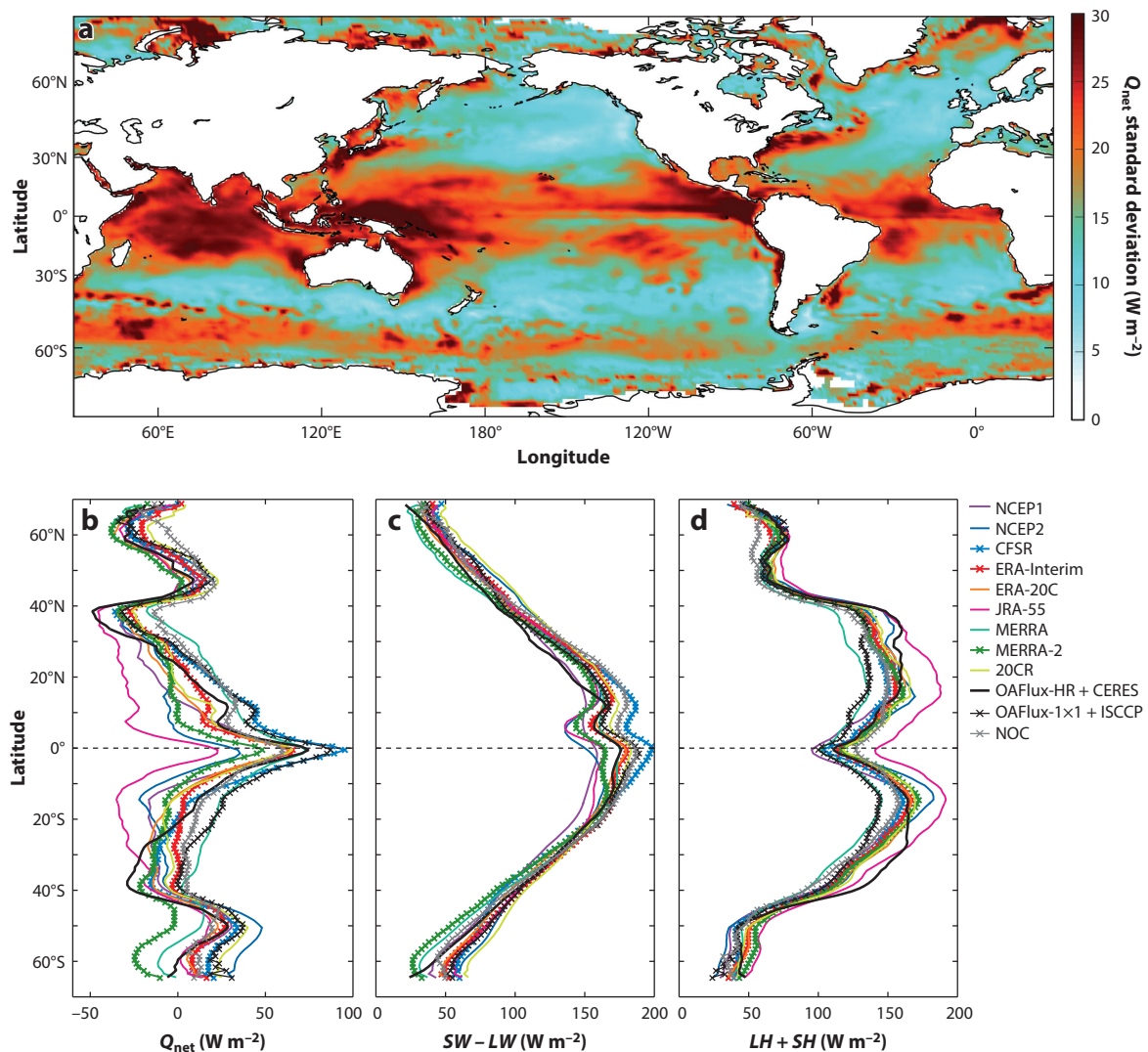


**Figure 4**

(a) Standard deviations between 12 mean  $Q_{\text{net}}$  products. The mean fields are constructed over the 10-year period of 2001–2010. (b–d) Zonal averages of  $Q_{\text{net}}$  (panel b),  $SW - LW$  (panel c), and  $LH + SH$  (panel d). Abbreviations: 20CR, Twentieth Century Reanalysis; CERES, Clouds and the Earth's Radiant Energy System—Energy Balanced and Filled; CFSR, Climate Forecast System Reanalysis; ERA-20C, European Centre for Medium-Range Weather Forecasts Twentieth Century; ERA-Interim, European Centre for Medium-Range Weather Forecasts Interim; ISCCP, International Satellite Cloud Climatology Project; JRA-55, Japanese 55-Year Reanalysis; MERRA, Modern-Era Retrospective Analysis for Research and Applications; NCEP, National Center for Environmental Prediction; NOC, National Oceanography Centre; OAFlux-1x1, 1°-gridded Objectively Analyzed Air–Sea Fluxes; OAFlux-HR, high-resolution (0.25°-gridded) Objectively Analyzed Air–Sea Fluxes.

(Figure 6a). The zonal averages reveal that the spread in the products is caused primarily by the gaps between two groups—the group that assimilates satellite scatterometers (i.e., CFSR, ERA-Interim, JRA-55, MERRA, MERRA-2, and OAFlux-HR) and the group that does not [NCEP2, European Centre for Medium-Range Weather Forecasts Twentieth Century (ERA-20C), and the

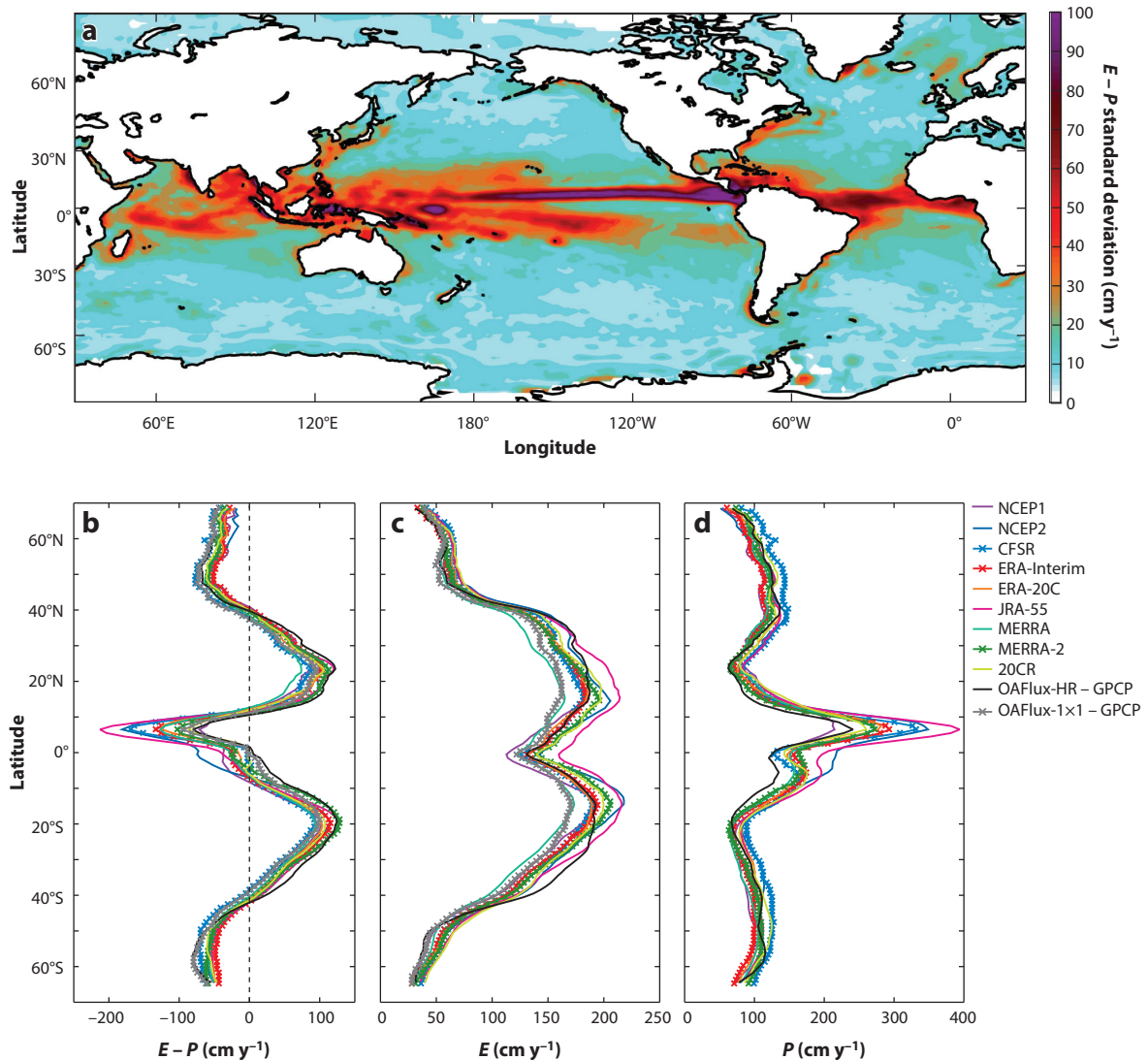


**Figure 5**

(a) Standard deviations between 11 mean  $E - P$  products. The mean fields are constructed over the 10-year period of 2001–2010. (b–d) Zonal averages of  $E - P$  (panel b),  $E$  (panel c), and  $P$  (panel d). Abbreviations: 20CR, Twentieth Century Reanalysis; CFSR, Climate Forecast System Reanalysis; ERA-20C, European Centre for Medium-Range Weather Forecasts Twentieth Century; ERA-Interim, European Centre for Medium-Range Weather Forecasts Interim; GPCP, Global Precipitation Climatology Project; JRA-55, Japanese 55-Year Reanalysis; MERRA, Modern-Era Retrospective Analysis for Research and Applications; NCEP, National Center for Environmental Prediction; OAFlux-1×1, 1°-gridded Objectively Analyzed Air-Sea Fluxes; OAFlux-HR, high-resolution (0.25°-gridded) Objectively Analyzed Air-Sea Fluxes.

Twentieth Century Reanalysis (20CR)]. Winds are vectors, and the zonal averages of  $\tau_x$  and  $\tau_y$  are not proportional to the zonal average of  $\tau$  due to the sign cancellation (**Figure 6b,c**).

## 2.6. Surface Budget Imbalance: Are CERES and GPCP Compatible Constraints?

Given the large uncertainties in surface flux estimates in the tropical and subtropical ocean, it is not a surprise that the surface energy and freshwater budgets determined by the mean  $Q_{\text{net}}$

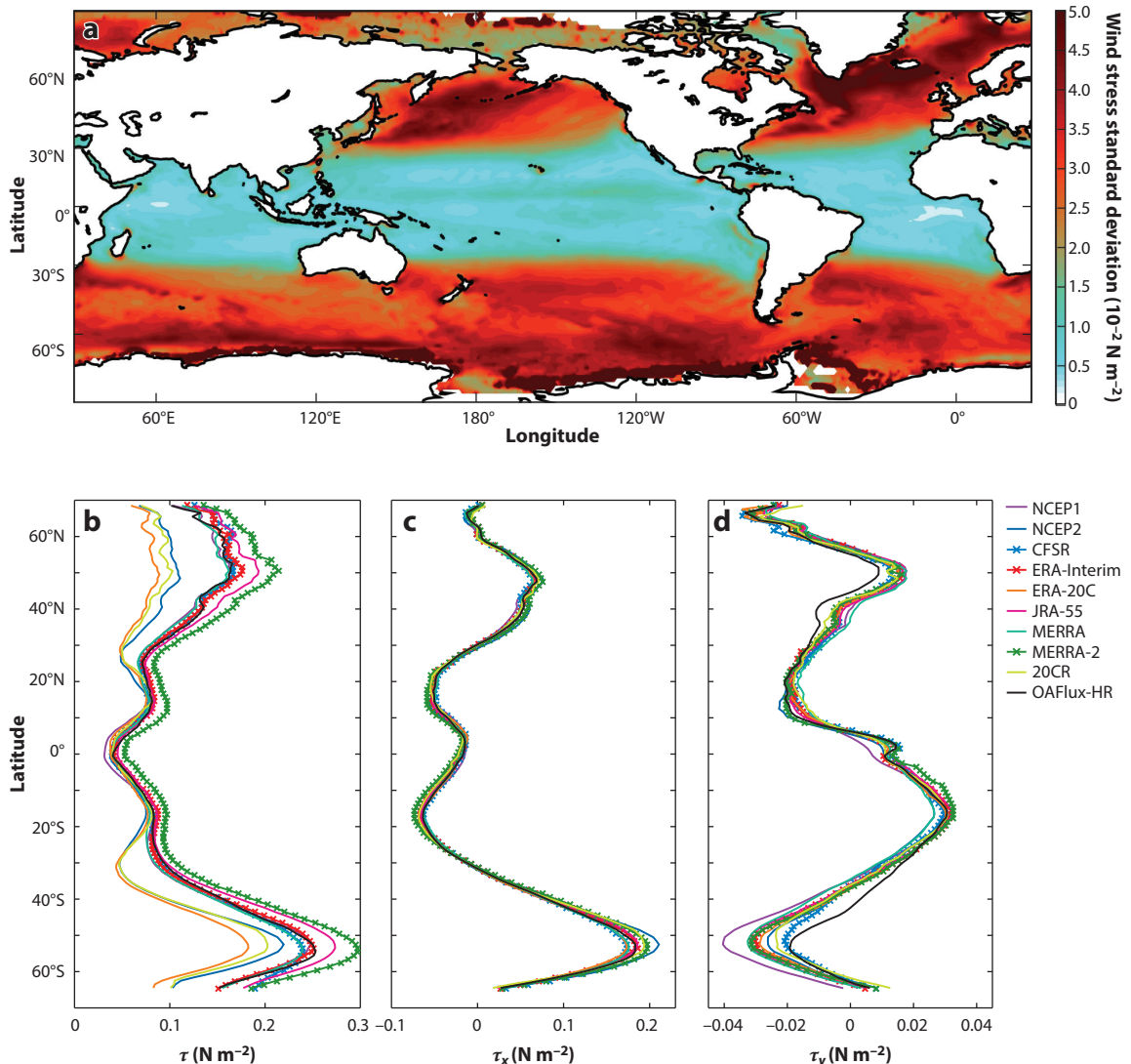


**Figure 6**

(a) Standard deviations between 10 mean wind stress magnitude ( $\tau$ ) products. The mean fields are constructed over the 10-year period of 2001–2010. (b–d) Zonal averages of wind stress magnitude (panel b), zonal wind stress (panel c), and meridional wind stress (panel d). Abbreviations: 20CR, Twentieth Century Reanalysis; CFSR, Climate Forecast System Reanalysis; ERA-20C, European Centre for Medium-Range Weather Forecasts Twentieth Century; ERA-Interim, European Centre for Medium-Range Weather Forecasts Interim; JRA-55, Japanese 55-Year Reanalysis; MERRA, Modern-Era Retrospective Analysis for Research and Applications; NCEP, National Center for Environmental Prediction; OAFlux-HR, high-resolution ( $0.25^\circ$ -gridded) Objectively Analyzed Air–Sea Fluxes.

product differ considerably from those determined by the  $E - P$  product (Figure 7a,b). The surface energy budget ranges from a significant ocean heat deficit of  $16 \text{ W m}^{-2}$  by JRA-55 to a significant ocean heat gain of  $25 \text{ W m}^{-2}$  by OAFlux-1 $\times$ 1. The surface freshwater budget ranges from a nearly perfect balance between  $E$  and  $P$  by CFSR to a large freshwater imbalance of  $27 \text{ cm y}^{-1}$  by the combined OAFlux-HR4 and GPCP. Interestingly, the product series of OAFlux affects

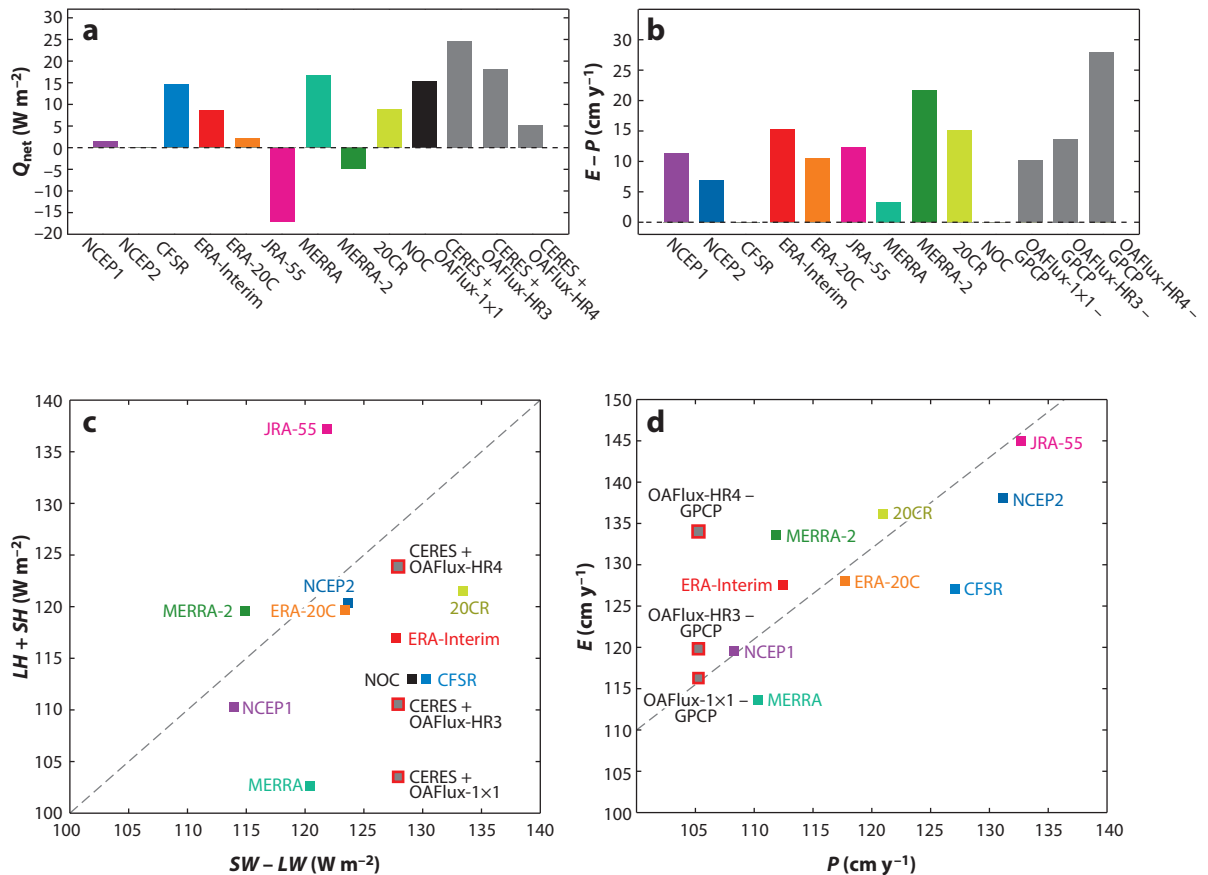


**Figure 7**

(a) Global-ocean mean energy ( $Q_{\text{net}}$ ) budget. (b) Global-ocean mean freshwater ( $E - P$ ) budget. (c) The ratio of the mean averages of  $SW - LW$  to  $LH + SH$ ; the dashed line denotes that this ratio equals 1.0. (d) The ratio of the mean averages of  $E$  to  $P$ ; the dashed line denotes that this ratio equals 1.1. Abbreviations: 20CR, Twentieth Century Reanalysis; CERES, Clouds and the Earth's Radian Energy System—Energy Balanced and Filled; CFSR, Climate Forecast System Reanalysis; ERA-20C, European Centre for Medium-Range Weather Forecasts Twentieth Century; ERA-Interim, European Centre for Medium-Range Weather Forecasts Interim; GPCP, Global Precipitation Climatology Project; JRA-55, Japanese 55-Year Reanalysis; MERRA, Modern-Era Retrospective Analysis for Research and Applications; NCEP, National Center for Environmental Prediction; NOC, National Oceanography Centre; OAFlux-1x1, 1°-gridded Objectively Analyzed Air–Sea Fluxes; OAFlux-HR3 and -HR4, high-resolution (0.25°-gridded) Objectively Analyzed Air–Sea Fluxes analysis computed from Coupled Ocean–Atmosphere Response Experiment (COARE) version 3 and version 4, respectively.

the surface energy and freshwater budget balance in the opposite way. While the imbalance in the energy budget is reduced from OAFlux-1x1 to OAFlux-HR3 to OAFlux-HR4, the imbalance in the freshwater budget is increased in the same order.

The scatter plots between  $SW - LW$  and  $LH + SH$  and between  $E$  and  $P$  (Figure 7c,d) shed some light on how the ocean and atmospheric flux components could be partitioned to achieve balanced budgets. As stated in Section 1, the energy budget determined from surface heat flux products is expected to achieve a closure within 2–3  $\text{W m}^{-2}$  due to the exclusion of polar regions. This implies that  $SW - LW$  should be balanced with  $LH + SH$  within this limit. Surface radiative budgets from CERES, NOC, ERA-Interim, and CFSR agree well with each other, but

the deviations in  $LH + SH$  set the total budgets apart. OAFlux-HR4 is a far better match for CERES than OAFlux-1×1. However, this works in the opposite way for the freshwater budget. On a long-term mean basis, the ocean freshwater budget should be balanced—that is,  $E - P - R \approx 0$  (Equation 7). If the  $E/P$  ratio is expressed in terms of  $E/P \approx (P + R)/P = 1 + R/P$ , one can expect that the larger (smaller) the ratio is, the more (less) continental runoff is needed to balance the water budget over the ocean. The  $E/P$  ratio is approximately 1.1 in most reanalysis products (Yu et al. 2017). OAFlux-1×1 and GPCP fall exactly on the line that delineates  $E/P = 1.1$  (**Figure 7d**), while OAFlux-HR4 is significantly off.

CERES and GPCP are community-standard products. The improvement made in OAFlux-HR4 improves the surface energy budget constrained by CERES but deteriorates the surface freshwater budget constrained by GPCP. The scatter relationships (**Figure 7c,d**) show that the CERES surface heat input is on the higher end and consistent with three reanalyses. By comparison, the GPCP freshwater input is the lowest among all reanalyses. Are GPCP and CERES pairwise compatible in terms of surface energy and freshwater budgets?

### 3. SUMMARY AND FUTURE PERSPECTIVES

This review has presented a perspective on the imbalance in surface energy and freshwater budgets using parameterization-based flux products and has attempted to draw attention to the problems and issues that arise when trying to balance the budgets from the ocean side. The views expressed here stem from my own decade-long research developing surface turbulent heat, moisture, and momentum fluxes from satellite observations. The inability to close the surface energy budget, despite the many efforts to improve the estimates of flux-related variables, has led me to reframe the thinking and attend to some questions that were seemingly straightforward but turned out to be difficult to address. In the end, the effectiveness of COARE v4 in improving surface turbulent heat flux estimates in the context of ocean energy and freshwater budgets is the most unexpected and yet promising outcome. It serves as a reminder that uncertainty remains not only in the flux-related variable estimation but also in parameterizing the behavior of turbulent transfer coefficients ( $c_e$ ,  $c_h$ , and  $c_d$ ) at all ranges of wind speeds.

Achieving globally balanced energy and freshwater budgets at the air-sea interface is a multi-faceted challenge, and I stress the importance of collaborations among various groups to understand and resolve discrepancies in the present-day turbulent flux estimates. These discrepancies include the differences between COARE algorithms and bulk flux parameterizations used in atmospheric reanalyses; differences in flux-related variables from VOS reports, satellite observations, and atmospheric reanalysis outputs; and differences between surface radiation and precipitation products in the context of surface energy and water cycles. There is a need for observers, flux product developers, and modelers to make concerted efforts to improve the flux observing system to meet the needs of developing and validating mean variables and flux algorithms.

### DISCLOSURE STATEMENT

The author is not aware of any affiliations, memberships, funding, or financial holdings that might be perceived as affecting the objectivity of this review.

### ACKNOWLEDGMENTS

This work was supported by funding from the NOAA Ocean Observing and Monitoring Division, NOAA Climate Reanalysis Task Force Team activity, and NASA Ocean Vector Winds Science

Team activity. X. Jin provided programming help. I thank J.B. Edson for providing the COARE v4 programming codes.

## LITERATURE CITED

- Adler RF, Huffman GJ, Chang A, Ferraro R, Xie P-P, et al. 2003. The version-2 Global Precipitation Climatology Project (GPCP) monthly precipitation analysis (1979–present). *J. Hydrometeorol.* 4:1147–67
- Allan RP, Liu C, Loeb NG, Palmer MD, Roberts M, et al. 2014. Changes in global net radiative imbalance 1985–2012. *Geophys. Res. Lett.* 41:5588–97
- Andersson A, Klepp C, Fennig K, Bakan S, Grassl H, Schulz J. 2011. Evaluation of HOAPS-3 ocean surface freshwater flux components. *J. Appl. Meteorol. Climatol.* 50:379–98
- Andreas EL, Edson JB, Monahan EC, Rouault M, Smith SD. 1995. The spray contribution to net evaporation from the sea: a review of recent progress. *Bound. Layer Meteorol.* 72:3–52
- Andreas EL, Persson POG, Hare JE. 2008. A bulk turbulent air-sea flux algorithm for high-wind, spray conditions. *J. Phys. Oceanogr.* 38:1581–96
- Bengtsson L, Hodges KI, Koumoutsaris S, Zahn M, Berrisford P. 2013. The changing energy balance of the polar regions in a warmer climate. *J. Clim.* 26:3112–29
- Bentamy A, Grodsky SA, Katsaros KB, Mestas-Nunñez AM, Blanke B, Desbiolles F. 2013. Improvement in air-sea flux estimates derived from satellite observations. *Int. J. Remote Sens.* 34:5243–61
- Bentamy A, Piolléa JF, Grouazel A, Danielsone R, Gulev S, et al. 2017. Review and assessment of latent and sensible heat flux accuracy over the global oceans. *Remote Sens. Environ.* 201:196–218
- Berry DI, Kent EC. 2011. Air-Sea fluxes from ICOADS: the construction of a new gridded dataset with uncertainty estimates. *Int. J. Climatol.* 31:987–1001
- Blanc TV. 1983. An error analysis of profile flux, stability, and roughness length measurements made in the marine atmospheric surface layer. *Bound. Layer Meteorol.* 26:243–67
- Bradley F, Fairall CW. 2007. *A guide to making climate quality meteorological and flux measurements at sea*. Tech. Memo. OAR PSD-311, Phys. Sci. Div., Earth Syst. Res. Lab., Natl. Ocean. Atmos. Adm., Boulder, CO
- Brunke MA, Fairall CW, Zeng X, Eymard L, Curry JA. 2003. Which bulk aerodynamic algorithms are least problematic in computing ocean surface turbulent fluxes? *J. Clim.* 16:619–35
- Chang H, Grossman RL. 1999. Evaluation of bulk surface flux algorithms for light wind conditions using data from the coupled ocean-atmosphere response experiment (COARE). *Q. J. R. Meteorol. Soc.* 125:1551–88
- Charnock H. 1955. Wind stress on a water surface. *Q. J. R. Meteorol. Soc.* 81:639–40
- Cheng L, Trenberth KE, Fasullo J, Boyer T, Abraham J, Zhu J. 2017. Improved estimates of ocean heat content from 1960 to 2015. *Sci. Adv.* 3:e1601545
- Chou S-H, Atlas RM, Shie C-L, Ardizzone J. 1995. Estimates of surface humidity and latent heat fluxes over oceans from SSM/I Data. *Mon. Weather Rev.* 123:2405–25
- Compo GP, Whitaker JS, Sardeshmukh PD, Matsui N, Allan RJ, et al. 2011. The Twentieth Century Reanalysis project. *Q. J. R. Meteorol. Soc.* 137:1–28
- Crawford TL, McMillen RT, Meyers TP, Hicks BB. 1993. Spatial and temporal variability of heat, water, vapor, carbon dioxide, and momentum air-sea exchange in a coastal environment. *J. Geophys. Res.* 98:12869–80
- Curry JA, Bentamy A, Bourassa MA, Bourras D, Bradley EF, et al. 2004. SEAFLUX. *Bull. Am. Meteorol. Soc.* 85:409–24
- da Silva AM, Young CC, Levitus S. 1994. *Atlas of Surface Marine Data*, Vol. 1: Algorithms and Procedures. NOAA Atlas NESDIS 6. Washington, DC: US Dep. Commerce
- DeCosmo J, Katsaros KB, Smith SD, Anderson RJ, Oost WA, et al. 1996. Air-sea exchange of water vapor and sensible heat: the Humidity Exchange Over the Sea Experiment (HEXOS) results. *Geophys. Res.* 101:12001–16
- Dee DP, Uppala SM, Simmons AJ, Berrisford P, Poli P, et al. 2011. The ERA-Interim reanalysis: configuration and performance of the data assimilation system. *Q. J. R. Meteorol. Soc.* 137:553–97
- Drennan WM, Gruber HC, Hauser D, Quentin C. 2003. On the wave age dependence of wind stress over pure wind seas. *J. Geophys. Res.* 108:8062

- Drennan WM, Zhang J, French JR, McCormick C, Black PG. 2007. Turbulent fluxes in the hurricane boundary layer. Part II: latent heat flux. *J. Atmos. Sci.* 64:1103–15
- Drijfhout SS, Blaker AT, Josey SA, Nurser AJG, Sinha B, Balmaseda MA. 2014. Surface warming hiatus caused by increased heat uptake across multiple ocean basins. *Geophys. Res. Lett.* 41:7868–74
- Edson JB. 2008. *Review of air-sea transfer processes*. Paper presented at the European Centre for Medium-Range Weather Forecasts (ECMWF) Workshop on Ocean-Atmosphere Interactions, Reading, UK, Nov. 10–12
- Edson JB, Hinton AA, Prada KE, Hare JE, Fairall CW. 1998. Direct covariance flux estimates from mobile platforms at sea. *J. Atmos. Ocean. Technol.* 15:547–62
- Edson JB, Jampana V, Weller RA, Bigorre SP, Plueddemann AJ, et al. 2013. On the exchange of momentum over the open ocean. *J. Phys. Oceanogr.* 43:1589–610
- Esbensen SK, Chelton DB, Vockers D, Sun J. 1993. An analysis of errors in Special Sensor Microwave Imager evaporation estimates over the global oceans. *J. Geophys. Res.* 98:7081–101
- Fairall CW, Barnier B, Berry DI, Bourassa MA, Bradley EF, et al. 2010. Observations to quantify air-sea fluxes and their role in climate variability and predictability. In *Proceedings of OceanObs'09: Sustained Ocean Observations and Information for Society*, Vol. 2: *Community White Papers*, ed. J Hall, DE Harrison, D Stammer, chap. 27. Paris: Eur. Space Agency
- Fairall CW, Bradley EF, Hare JE, Grachev AA, Edson JB. 2003. Bulk parameterization of air-sea fluxes: updates and verification for the COARE algorithm. *J. Clim.* 16:571–91
- Fairall CW, Bradley EF, Rogers DP, Edson JB, Young GS. 1996. Bulk parameterization of air-sea fluxes for TOGA COARE. *J. Geophys. Res.* 101:3747–64
- Fairall CW, Larsen SE. 1986. Inertial dissipation methods and turbulent fluxes at the air ocean interface. *Bound. Layer Meteorol.* 34:287–301
- Føre I, Kristjansson JE, Kolstad EW, Bracegirdle TJ, Saetra Ø, Røsting B. 2012. A ‘hurricane-like’ polar low fuelled by sensible heat flux: high-resolution numerical simulations. *Q. J. R. Meteorol. Soc.* 138:1308–24
- Garratt JR. 1977. Review of drag coefficients over oceans and continents. *Mon. Weather Rev.* 105:915–29
- Grachev AA, Fairall CW, Hare JE, Edson JB, Miller SD. 2003. Wind stress vector over ocean waves. *J. Phys. Oceanogr.* 33:2408–29
- Grist JP, Josey SA. 2003. Inverse analysis of the SOC air-sea flux climatology using ocean heat transport constraints. *J. Clim.* 16:3274–95
- Gulev SK, Belyaev K. 2012. Probability distribution characteristics for surface air-sea turbulent heat fluxes over the global ocean. *J. Clim.* 25:184–206
- Gulev SK, Josey SA, Bourassa M, Breivik L-A, Cronin MF, et al. 2010. Surface energy and CO<sub>2</sub> fluxes in the Global Ocean-Atmosphere-Ice System. In *Proceedings of OceanObs'09: Sustained Ocean Observations and Information for Society*, Vol. 1: *Plenary Papers*, ed. J Hall, DE Harrison, D Stammer, chap. 19. Paris: Eur. Space Agency
- Hansen J, Nazarenko L, Ruedy R, Sato M, Willis J, et al. 2005. Earth’s energy imbalance: confirmation and implications. *Science* 308:1431–35
- Hwang PA. 2005. Temporal and spatial variation of the drag coefficient of a developing sea under steady wind-forcing. *J. Geophys. Res.* 110:C07024
- Isemer H, Willebrand J, Hasse L. 1989. Fine adjustment of large-scale air-sea energy flux parameterizations by direct estimates of ocean heat transport. *J. Clim.* 2:1173–84
- Jackson DL, Wick GA, Bates JJ. 2006. Near-surface retrieval of air temperature and specific humidity using multi-sensor microwave satellite observations. *J. Geophys. Res.* 111:D10306
- Janssen P. 2008. *Air-sea interaction through waves*. Paper presented at the European Centre for Medium-Range Weather Forecasts (ECMWF) Workshop on Ocean-Atmosphere Interactions, Reading, UK, Nov. 10–12
- Jin X, Yu L. 2013. Assessing high-resolution analysis of surface heat fluxes in the Gulf Stream region. *J. Geophys. Res. Oceans* 118:5353–75
- Jin X, Yu L, Jackson DL, Wick GA. 2015. An improved near-surface specific humidity and air temperature climatology for the SSM/I satellite period. *J. Atmos. Ocean. Technol.* 32:412–33
- Josey SA, Gulev SK, Yu L. 2013. Exchanges through the ocean surface. In *Ocean Circulation and Climate: A 21st Century Perspective*, ed. G Siedler, S Griffies, J Gould, J Church, pp. 115–40. Oxford, UK: Academic. 2nd ed.

- Josey SA, Kent EC, Taylor PK. 1999. New insights into the ocean heat budget closure problem from analysis of the SOC air-sea flux climatology. *J. Clim.* 12:2856–80
- Kalnay E, Kanamitsu M, Kistler R, Collins W, Deaven D, et al. 1996. The NMC/NCAR 40-year reanalysis project. *Bull. Am. Meteorol. Soc.* 77:437–71
- Kanamitsu M, Ebisuzaki W, Woollen J, Yang S-K, Hnilo JJ, et al. 2002. NCEP-DOE AMIP-II reanalysis (R-2). *Bull. Am. Meteorol. Soc.* 83:1631–43
- Kato S, Loeb NG, Rose FG, Doelling DR, Rutan DA, et al. 2013. Surface irradiances consistent with CERES-derived top-of-atmosphere shortwave and longwave irradiances. *J. Clim.* 26:2719–40
- Kobayashi S, Ota Y, Harada Y, Ebita A, Moriya M, et al. 2015. The JRA-55 reanalysis: general specifications and basic characteristics. *J. Meteorol. Soc. Jpn.* 93:5–48
- Kubota M, Ichikawa K, Iwasaka N, Kizu S, Konda M, Kutsuwada K. 2002. Japanese ocean flux data sets with use of remote sensing observations (J-OFURO). *J. Oceanogr.* 58:213–15
- Landwehr S, O’Sullivan N, Ward B. 2015. Direct flux measurements from mobile platforms at sea: motion and airflow distortion corrections revisited. *J. Atmos. Ocean. Technol.* 32:1163–78
- Large WG, Danabasoglu G, Doney SC, McWilliams JC. 1997. Sensitivity to surface forcing and boundary layer mixing in a global ocean model: annual mean climatology. *J. Phys. Oceanogr.* 27:2418–47
- Large WG, Pond S. 1981. Open ocean momentum flux measurements in moderate to strong winds. *J. Phys. Oceanogr.* 11:324–36
- Large WG, Yeager SG. 2009. The global climatology of an interannually varying air-sea flux data set. *Clim. Dyn.* 33:341–64
- Levitus S, Antonov J, Boyer T, Stephens C. 2005. Warming of the world ocean, 1955–2003. *Geophys. Res. Lett.* 32:L02604
- Liu C, Liu C, Allan RP, Mayer M, Hyder P, et al. 2017. Evaluation of satellite and reanalysis-based global net surface energy flux and uncertainty estimates. *J. Geophys. Res. Atmos.* 122:6250–72
- Liu WT. 1988. Moisture and latent heat flux variabilities in the tropical Pacific derived from satellite data. *J. Geophys. Res.* 93:6749–60
- Liu WT, Katsaros KB, Businger JA. 1979. Bulk parameterization of air-sea exchanges of heat and water vapor including the molecular constraints at the interface. *J. Atmos. Sci.* 36:1722–35
- Loeb NG, Doelling DR, Wang H, Su W, Nguyen C, et al. 2018. Clouds and the Earth’s Radiant Energy System (CERES) Energy Balanced and Filled (EBAF) Top-of-Atmosphere (TOA) Edition-4.0 data product. *J. Clim.* 31:895–918
- Loeb NG, Lyman JM, Johnson GC, Allan RP, Doelling DR, et al. 2012. Observed changes in top-of-the-atmosphere radiation and upper-ocean heating consistent within uncertainty. *Nat. Geosci.* 5:110–113
- Louis JF. 1979. A parametric model of vertical eddy fluxes in the atmosphere. *Bound. Layer Meteorol.* 17:187–202
- Lyman JM, Johnson GC. 2013. Estimating global ocean heat content changes in the upper 1800 m since 1950 and the influence of climatology choice. *J. Clim.* 27:1945–57
- Miller MJ, Beljaars ACM, Palmer TN. 1992. The sensitivity of the ECMWF model to the parameterization of evaporation from the tropical oceans. *J. Clim.* 5:418–34
- Molod A, Takacs L, Suarez M, Bacmeister J. 2015. Development of the GEOS-5 atmospheric general circulation model: evolution from MERRA to MERRA2. *Geosci. Model Dev.* 8:1339–56
- Monin AS, Obukhov AM. 1954. Basic regularity in turbulent mixing in the surface layer of the atmosphere. *Tr. Geofiz. Inst. Akad. Nauk SSSR* 24:163–87
- Newman M, Sardeshmukh PD, Bergman JW. 2000. An assessment of the NCEP, NASA, and ECMWF reanalyses over the tropical west Pacific warm pool. *Bull. Am. Meteorol. Soc.* 81:41–48
- Paulson CA, Leavitt E, Fleagle RG. 1972. Air-sea transfer of momentum, heat and water determined from profile measurements during BOMEX. *J. Phys. Oceanogr.* 2:487–97
- Poli P, Hersbach H, Tan DGH, Dee DP, Thépaut J-N, et al. 2013. *The data assimilation system and initial performance evaluation of the ECMWF pilot reanalysis of the 20th-century assimilating surface observations only (ERA-20C)*. ERA Rep. Ser. 14, Eur. Cent. Medium-Range Weather Forecasts, Reading, UK
- Powell MD, Vickery PJ, Reinhold TA. 2003. Reduced drag coefficient for high wind speeds in tropical cyclones. *Nature* 422:279–83
- Prytherch J, Kent EC, Fangohr S, Berry DI. 2014. A comparison of SSM/I-derived global marine surface-specific humidity datasets. *Int. J. Climatol.* 35:2359–81

- Rienecker MM, Suarez MJ, Gelaro R, Todling R, Bacmeister J, et al. 2011. MERRA: NASA's modern-era retrospective analysis for research and applications. *J. Clim.* 24:3624–48
- Roberts JB, Clayson CA, Robertson FR, Jackson D. 2010. Predicting near-surface characteristics from SSM/I using neural networks with a first guess approach. *J. Geophys. Res.* 115:D19113
- Rosenfeld D, Lensky IM. 1998. Satellite-based insights into precipitation formation processes in continental and maritime convective clouds. *Bull. Am. Meteorol. Soc.* 79:2457–76
- Saha S, Moorthi S, Pan H-L, Wu X, Wang J, et al. 2010. The NCEP Climate Forecast System Reanalysis. *Bull. Am. Meteorol. Soc.* 91:1015–57
- Schlüssel P, Schanz L, Englisch G. 1995. Retrieval of latent-heat flux and longwave irradiance at the sea-surface from SSM/I and AVHRR measurements. *Adv. Space Res.* 16:107–16
- Schulz J, Schlüssel P, Grassl H. 1993. Water vapour in the atmospheric boundary layer over oceans from SSM/I measurements. *Int. J. Remote Sens.* 14:2773–89
- Serreze MC, Barrett AP, Slater AG, Steele M, Zhang J, Trenberth KE. 2007. The large-scale energy budget of the Arctic. *J. Geophys. Res.* 112:D11122
- Simonot J-YR, Gautier C. 1989. Satellite estimates of surface evaporation in the Indian Ocean during the 1979 monsoon. *Ocean-Air Interact.* 1:239–56
- Smith SD. 1988. Coefficients for sea surface wind stress, heat flux, and wind profiles as a function of wind speed and temperature. *J. Geophys. Res.* 93:15467–15472
- Soloviev A, Lukas R, Donelan M, Haus B, Ginis I. 2014. The air-sea interface and surface stress under tropical cyclones. *Sci. Rep.* 4:5306
- Stephens GL, Li J, Wild M, Clayson CA, Loeb N, et al. 2012. An update on Earth's energy balance in light of the latest global observations. *Nat. Geosci.* 5:691–96
- Trenberth KE, Caron JM. 2001. Estimates of meridional atmosphere and ocean heat transports. *J. Clim.* 14:3433–43
- Trenberth KE, Fasullo JT, Balmaseda MA. 2014. Earth's energy imbalance. *J. Clim.* 27:3129–44
- Valdivieso M, Haines K, Balmaseda M, Chang Y-S, Drevillon M, et al. 2017. An assessment of air-sea heat fluxes from ocean and coupled reanalyses. *Clim. Dyn.* 49:983–1008
- von Schuckmann K, Palmer MD, Trenberth KE, Cazenave A, Chambers D, et al. 2016. An imperative to monitor Earth's energy imbalance. *Nat. Clim. Change* 6:138–44
- WCRP (World Clim. Res. Programme). 1989. *WOCE surface flux determinations: a strategy for in situ measurements*. WMO Tech. Doc. 304, WCRP-23, World Meteorol. Organ., Geneva
- Webster PA, Lukas R. 1992. TOGA COARE: the Coupled Ocean-Atmosphere Response Experiment. *Bull. Am. Meteorol. Soc.* 73:1377–416
- Weller RA, Bradley EF, Edson JB, Fairall CW, Brooks I, et al. 2008. Sensors for physical fluxes at the sea surface: energy, heat, water, salt. *Ocean Sci.* 4:247–63
- Weller RA, Bradley F, Lukas R. 2004. The interface or air-sea flux component of the TOGA Coupled Ocean-Atmosphere Response Experiment and its impact on subsequent air-sea interaction studies. *J. Atmos. Ocean. Technol.* 21:223–57
- WGASF (Work. Group Air-Sea Fluxes). 2000. *Intercomparison and validation of ocean-atmosphere energy flux fields: final report of the Joint WCRP/SCOR Working Group on Air-Sea Fluxes (WGASF)*. WMO Tech. Doc. 1036, WCRP-112, World Meteorol. Organ., Geneva
- Wild M, Folini D, Schar C, Loeb N, Dutton EG, König-Langlo G. 2013. The global energy balance from a surface perspective. *Clim. Dyn.* 40:3107–34
- Wunsch C. 2005. The total meridional heat flux and its oceanic and atmospheric partition. *J. Clim.* 18:4374–80
- Yu L, Haines K, Bourassa M, Cronin M, Gulev S, et al. 2013. *Towards achieving global closure of ocean heat and freshwater budgets: recommendations for advancing research in air-sea fluxes through collaborative activities*. Report of the CLIVAR/GSOP/WHOI Workshop on Ocean Syntheses and Surface Flux. WCRP Informal/Ser. Rep. 13/2013, ICPO Informal Rep. 189/13, Int. CLIVAR Proj. Off., China
- Yu L, Jin X. 2012. Buoy perspective of a high-resolution global ocean vector wind analysis using passive radiometers and active scatterometers from 1987 to the present. *J. Geophys. Res. Oceans* 117:C11013
- Yu L, Jin X. 2014. Insights on the OAFlux ocean surface vector wind analysis merged from scatterometers and passive microwave radiometers (1987 onward). *J. Geophys. Res. Oceans* 119:5244–69

- Yu L, Jin X. 2018. Retrieving near-surface air humidity and temperature using a regime-dependent regression model. *Remote Sens. Environ.* 215:199–216
- Yu L, Jin X, Josey SA, Lee T, Kumar A, et al. 2017. The global ocean water cycle in atmospheric reanalysis, satellite, and ocean salinity. *J. Clim.* 30:3829–52
- Yu L, Jin X, Weller RA. 2008. *Multidecade global flux datasets from the Objectively Analyzed Air-sea Fluxes (OAFlux) project: latent and sensible heat fluxes, ocean evaporation, and related surface meteorological variables*. OAFlux Proj. Tech. Rep. OA-2008-01, Woods Hole Oceanogr. Inst., Woods Hole, MA
- Yu L, Weller RA. 2007. Objectively Analyzed air-sea heat Fluxes (OAFlux) for the global ocean. *Bull. Am. Meteorol. Soc.* 88:527–39
- Zeng X, Zhao M, Dickinson RE. 1998. Intercomparison of bulk aerodynamic algorithms for the computation of sea surface fluxes using TOGA COARE and TAO data. *J. Clim.* 11:2628–44

# Contents

## Passing the Baton to the Next Generation: A Few Problems

That Need Solving

*Cindy Lee* ..... 1

## A Conversation with Walter Munk

*Walter Munk and Carl Wunsch* ..... 15

## Compound-Specific Isotope Geochemistry in the Ocean

*Hilary G. Close* ..... 27

## Mechanisms and Pathways of Small-Phytoplankton Export from the Surface Ocean

*Tammi L. Richardson* ..... 57

## Using Noble Gases to Assess the Ocean's Carbon Pumps

*Roberta C. Hamme, David P. Nicholson, William J. Jenkins,  
and Steven R. Emerson* ..... 75

## Biogeochemical Controls on Coastal Hypoxia

*Katja Fennel and Jeremy M. Testa* ..... 105

## Planktonic Marine Archaea

*Alyson E. Santoro, R. Alexander Richter, and Christopher L. Dupont* ..... 131

## The Variable Southern Ocean Carbon Sink

*Nicolas Gruber, Peter Landschützer, and Nicole S. Lovenduski* ..... 159

## Arctic and Antarctic Sea Ice Change: Contrasts, Commonalities, and Causes

*Ted Maksym* ..... 187

## Biologically Generated Mixing in the Ocean

*Eric Kunze* ..... 215

## Global Air–Sea Fluxes of Heat, Fresh Water, and Momentum:

Energy Budget Closure and Unanswered Questions

*Lisan Yu* ..... 227

## The Global Overturning Circulation

*Paola Cessi* ..... 249

The Water Mass Transformation Framework for Ocean Physics and Biogeochemistry	
<i>Sjoerd Groeskamp, Stephen M. Griffies, Daniele Iudicone, Robert Marsh, A.J. George Nurser, and Jan D. Zika</i>	271
Climate Change, Coral Loss, and the Curious Case of the Parrotfish Paradigm: Why Don't Marine Protected Areas Improve Reef Resilience?	
<i>John F. Bruno, Isabelle M. Côté, and Lauren T. Toth</i>	307
Marine Environmental Epigenetics	
<i>Jose M. Eirin-Lopez and Hollie M. Putnam</i>	335
Marine Metazoan Modern Mass Extinction: Improving Predictions by Integrating Fossil, Modern, and Physiological Data	
<i>Piero Calosi, Hollie M. Putnam, Richard J. Twitchett, and Fanny Vermandele</i>	369
Partnering with Fishing Fleets to Monitor Ocean Conditions	
<i>Glen Gawarkiewicz and Anna Malek Mercer</i>	391
The Scientific Legacy of the CARIACO Ocean Time-Series Program	
<i>Frank E. Muller-Karger, Yrene M. Astor, Claudia R. Benitez-Nelson, Kristen N. Buck, Kent A. Fanning, Laura Lorenzoni, Enrique Montes, Digna T. Rueda-Roa, Mary I. Scranton, Eric Tappa, Gordon T. Taylor, Robert C. Thunell, Luis Troccoli, and Ramon Varela</i>	413
Unoccupied Aircraft Systems in Marine Science and Conservation	
<i>David W. Johnston</i>	439
Windows into Microbial Seascapes: Advances in Nanoscale Imaging and Application to Marine Sciences	
<i>Gordon T. Taylor</i>	465
The Formation and Distribution of Modern Ooids on Great Bahama Bank	
<i>Paul (Mitch) Harris, Mara R. Diaz, and Gregor P. Eberli</i>	491

## Errata

An online log of corrections to *Annual Review of Marine Science* articles may be found at <http://www.annualreviews.org/errata/marine>